Journal of Nuclear Medicine, published on April 13, 2020 as doi:10.2967/jnumed.120.241877

Biodistribution of a CD3/EpCAM bispecific T-cell engager is driven by the CD3 arm

Frans V. Suurs[1], Grit Lorenczewski[2], Sabine Stienen[2], Matthias Friedrich[2], Elisabeth G.E. de Vries[1], Derk Jan A. de Groot[1] and Marjolijn N. Lub-de Hooge[3].

[1]Department of Medical Oncology, University Medical Center Groningen, Groningen, the Netherlands; [2]Amgen Research Munich GmbH, Munich, Germany; [3]Department of Clinical Pharmacy and Pharmacology, University Medical Center Groningen, Groningen, the Netherlands;

Corresponding author:

M.N. Lub-de Hooge, PharmD, PhD, Department of Clinical Pharmacy and Pharmacology, University Medical Center Groningen, University of Groningen, PO Box 30.001, 9700 RB Groningen, The Netherlands. +31503614071 (phone); +31503614087 (fax); m.n.de.hooge@umcg.nl (e-mail).

Running Title: Biodistribution of ^{89}Zr-BiTE molecules

Word count: 5049

Disclosure of Potential Conflicts of Interest: The work performed in this study is co-financed by the PPP-subsidy of the Top consortia for Knowledge and Innovation of the Ministry of Economic Affairs. G. Lorenczewski holds ownership interests in Amgen. S. Stienen holds ownership interest (including patents) in Amgen. M. Friedrich holds

ownership interest (including patents) in Amgen. E.G.E de Vries reports Institutional Financial Support for her advisory role from Sanofi, Pfizer, Daiichi Sankyo, NSABP, Merck and Institutional Financial Support for clinical trials or contracted research from Amgen, Genentech, Roche, Chugai Pharma, Synthon, CytomX Therapeutics, Nordic Nanovector, Regeneron, G1 Therapeutics, AstraZeneca, Radius Health, Bayer.
No potential conflicts of interest were disclosed by the other authors.

ABSTRACT

BiTE® (Bispecific T-cell engager) molecules are designed to engage and activate cytotoxic T-cells to kill tumor cells. Little is known about their biodistribution in immunocompetent settings. To explore their pharmacokinetics and the role of the immune cells, BiTE molecules were radiolabeled with positron emission tomography (PET) isotope zirconium-89 (^{89}Zr) and studied in immunocompetent and immunodeficient mouse models.

PET images and *ex-vivo* biodistribution in immunocompetent mice with [^{89}Zr]Zr-DFO-*N*-suc-muS110, targeting mouse CD3 (K_d = 2.9 nM) and mouse epithelial cell adhesion molecule (EpCAM; K_d = 21 nM), and [^{89}Zr]Zr-DFO-*N*-suc-hyS110, targeting only mouse CD3 (K_d = 2.9 nM), showed uptake in tumor, spleen and other lymphoid organs, while the human-specific control BiTE [^{89}Zr]Zr-DFO-*N*-suc-AMG 110 showed similar tumor uptake but lacked spleen uptake.

[^{89}Zr]Zr-DFO-*N*-suc-muS110 spleen uptake was lower in immunodeficient than in immunocompetent mice. After repeated administration of non-radiolabeled muS110 to immunocompetent mice ^{89}Zr-muS110 uptake in spleen, and other lymphoid tissues, decreased and was comparable to uptake in immunodeficient mice, indicating saturation of CD3 binding sites.

Autoradiography and immunohistochemistry demonstrated colocalization of [^{89}Zr]Zr-DFO-*N*-suc-muS110 and [^{89}Zr]Zr-DFO-*N*-suc-hyS110 with CD3-positive T-cells in the tumor and spleen but not with EpCAM expression. Also, uptake in the duodenum correlated with a high incidence of T-cells.

Conclusion: [^{89}Zr]Zr-DFO-*N*-suc-muS110 biodistribution is mainly dependent on the T-cell targeting arm with limited contribution of its second arm, targeting EpCAM. These findings highlight the need for extensive biodistribution studies of novel bispecific constructs as results might have implications for their respective drug development and clinical translation.

Keywords: Bispecific T-cell engager (BiTE) molecule, PET-imaging, syngeneic mouse model, oncology, cancer-immunotherapy

INTRODUCTION

Impressive results with immunotherapy across various cancer types have greatly increased confidence in modulation of the immune system as a treatment for cancer. Currently, several immune checkpoint inhibiting monoclonal antibodies are registered for cancer treatment. Also, numerous modified monoclonal antibodies are being studied with the aim to improve antitumor efficacy (*1*). Among them are BiTE® (bispecific T-cell engagers) molecules which are 53 kDa antibody constructs consisting of two single-chain variable fragments on one peptide chain (*2*). One single-chain variable fragment binds to T-cells via the CD3 receptor, the other single-chain variable fragment binds to the tumor cell via a tumor-associated antigen. When the BiTE molecule binds to both cell types, a cytolytic synapse is formed resulting in perforin and granzyme-B release and eventually tumor cell killing (*3-5*).

Blinatumomab, a BiTE molecule targeting CD19 and CD3, is approved by the Food and Drug Administration and European Medicine Agency for the treatment of Philadelphia chromosome negative B cell acute lymphoblastic leukemia (ALL). In a phase 1 trial patients with relapsed or refractory acute myeloid leukemia were treated with AMG 330, a BiTE molecule targeting CD33 and CD3. Two patients out of 35 had a complete response and two patients had a complete response with incomplete hematologic recovery (*6*).

In addition, several BiTE molecules for both solid tumors and hematologic malignancies are currently in development (*7,8*). In solid tumors, few clinical results have been published to date (*7,9*). Preclinical positron emission tomography (PET)-imaging studies with BiTE molecules showed specific tumor uptake in immunodeficient mice

bearing solid human tumors (*10,11*). No uptake in lymphoid organs was seen. However, evaluating the role of the CD3-targeting arm on the distribution or accessibility was not possible since human-specific BiTE molecules were used. Recently, a first small clinical PET-imaging study was performed with zirconium-89 (^{89}Zr)-labeled AMG 211, a BiTE molecule targeting CD3 and carcinoembryonic antigen (CEA). Here, heterogeneous tumor uptake within and between patients as well as uptake in lymphoid tissue was shown (*12*).

Epithelial cell adhesion molecule (EpCAM) is expressed by many epithelial tumors (*13*) and muS110, a BiTE molecule targeting mouse EpCAM and mouse CD3 reduced tumor growth in mice (*14*). This murine BiTE molecule mus110 allowed us to study its biodistribution in a syngeneic mouse model, best reflecting the human situation. To evaluate the influence of the T-cell targeting arm and the EpCAM targeting arm on the whole body biodistribution of this BiTE molecule we performed a PET-imaging study with [^{89}Zr]Zr-DFO-*N*-suc-BiTE molecules in immunocompetent and immunodeficient mouse models.

MATERIALS AND METHODS

BiTE Molecules and Cell Lines

BiTE molecules were provided by Amgen. MuS110 binds to mouse CD3ε and mouse EpCAM, hyS110 to mouse CD3ε and human EpCAM and AMG 110 to human CD3ε and human EpCAM. Production of these BiTE molecules has been described (*14,15*). Their molecular weight is approximately 53kDa. Dissociation constants of

muS110 are 2.9 nM and 21 nM for mouse CD3 and mouse EpCAM, respectively (*14*). The mouse CD3-targeting arm of muS110 is used for hyS110 as well.

MuS110, hyS110 and AMG 110 were purified from buffer excipients using a Vivaspin-500 30 kDa filter (Sartorius) and formulation buffer was changed to NaCl 0.9% (Braun). Tetrafluorphenol-N-succinyldesferrioxamine-B (TFP-*N*-suc-Df-Fe; ABX) was conjugated to muS110, hyS110 and AMG 110 resulting in a protein:chelator end ratio of 1:6, 1:6 and 1:3, respectively. Conjugation has been described previously (*16*). Conjugation efficiency and formation of aggregates were evaluated by size exclusion high performance liquid chromatography (SE-HPLC, Waters) using a Superdex 75 column (GE Healthcare) and PBS (140 mmol/L NaCl, 9 mmol/L Na_2HPO_4, 1.3 mmol/L NaH_2PO_4; pH 7.4) as mobile phase. No visible particles were detected.

After purification by dialysis with slide-a-lyzer cassettes, 10 kDa filter (ThermoFischer Scientific), the conjugate was stored at 1 mg/mL at -80 ^{o}C. Stability and immunoreactivity were evaluated by HPLC analysis and by cell based binding assays, respectively. In binding assays increasing concentrations of conjugated or unmodified BiTE molecules were incubated with human or murine T-cells or human or murine EpCAM+ B16/F10 tumor cells. Maintained immunoreactivity was further evaluated by adding increasing concentrations of conjugated or unmodified muS110 to fixed concentrations of murine T-cells in the presence of murine EpCAM+ B16/F10 tumor cells in a ratio of 1:10. Read-outs were propidium iodide-positive tumor cells for cytotoxicity, and CD69-positive (BD Biosciences; 553237) and CD25-positive (BD Biosciences; 553237) T-cells for T-cell activation. Murine and human T-cells were obtained by negative selection with the Pan T Cell Isolation Kit II, mouse (Miltenyi Biotec) or the Pan T Cell

Isolation Kit, human (Miltenyi Biotec), respectively. Data was acquired by FACS Canto II (BD Biosciences) and binding curves were read-out by median fluorescence intensity (MFI) on FACS Diva (BD Biosciences) software.

The conjugated BiTE molecules were labeled with ^{89}Zr (*16*) with a specific activity of 400-500 MBq/mg. Radiochemical purity was evaluated by a trichloroacetic acid precipitation assay, all tracers had a radiochemical purity of > 95%.

The murine mammary carcinoma cell line 4T1 (American Type Culture Collection) is EpCAM-positive and was cultured in RPMI-1640 medium (Invitrogen) containing 10% fetal calf serum (FCS, Bodinco BV). B16/F10 tumor cells transfected with human EpCAM were cultured in DMEM medium (Biochrom) containing 10% FCS (Invitrogen). B16/F10 tumor cells transfected with murine EpCAM were cultured in DMEM medium containing 10% FCS (Invitrogen) and 600 U/mL G418 (Millipore).

Cells were used between passages 5-20 after thawing and were routinely tested for mycoplasma. All cells were cultured under aseptic conditions at 37°C in an incubator providing humidified atmosphere of 5% CO_2 in air.

Animal Experiments

Animal experiments were approved by the Institutional Animal Care and Use Committee of the University of Groningen. Female BALB/c mice (8-10 weeks old, BALB/cOlaHsd, Envigo), from now on referred to as immunocompetent, and female nude BALB/c (BALB/cOlaHsd-*Foxn1*^{nu}, Envigo), from now on referred to as immunodeficient, were acclimatized for 1 week. All mice were housed in groups of 3-6 per cage. Immunocompetent mice were housed complying with FELASA 2014 guidelines. Immunodeficient mice were housed in individually ventilated cages. Where possible, mice

were allocated randomly to tracer groups. The mice were injected with 5 x 10^4 4T1 tumor cells in 50 µL RPMI-1640, containing phenol red, in the lower mammary fat pad. To prevent toxicity of the tracer dose (10 µg), mice received low-dose muS110 (0.2 µg) intravenously (iv) daily for 5 days prior to tracer injection. Previously observed muS110 side effects, leading to cytokine release, appeared dependent on EpCAM+ B and T-cells in the circulation, and depleting these cells with low-dose muS110 increased muS110 tolerance of these mice (*17*). In addition, after the low-dose muS110 administration a group of BALB/c mice (BALB/cOlaHsd) received 10 µg muS110 bolus iv daily for another 5 days to assess possible target saturation. This group will be referred to as repeated muS110 administration group.

The tracers, 10 µg [^{89}Zr]Zr-DFO-*N*-suc-BiTE molecules, were injected iv in the tail vein when tumors reached ± 200 mm^3. Mice were anesthetized with isoflurane/medical air inhalation (5% induction, 2.5% maintenance) during injections and PET-imaging. First, the *in-vivo* biodistribution over time of 10 µg [^{89}Zr]Zr-DFO-*N*-suc-muS110 in 4T1-bearing immunocompetent mice was visualized by microPET scanning performed at 0.5, 3, 6, 24, 48 and 72 hours after injection. MicroPET scans were acquired as described before with the Focus220 rodent scanner (CTI Siemens) (*10*).

Second, biodistribution of 10 µg [^{89}Zr]Zr-DFO-*N*-suc-muS110, [^{89}Zr]Zr-DFO-*N*-suc-hys110 and [^{89}Zr]Zr-DFO-*N*-suc-AMG 110 was compared in 4T1-bearing immunocompetent mice 24 hours after iv tracer injection by PET-imaging followed by *ex-vivo* biodistribution. This procedure was repeated for 10 µg [^{89}Zr]Zr-DFO-*N*-suc-muS110 and [^{89}Zr]Zr-DFO-*N*-suc-AMG 110 in 4T1-bearing immunodeficient mice and to the

repeated mus110 administration mice. Again, all mice underwent PET scans 24 hours after iv tracer administration followed by *ex-vivo* biodistribution.

Organs of interest were weighed and measured in a calibrated Wizard gamma counter (PerkinElmer). Counts of known standards were used to convert counts into injected dose. Tissue activity is expressed as percentage injected dose per gram (%ID/g). Relevant tissues were fixed in formalin (4% paraformaldehyde /PBS) for 1 to 3 days or stored at -80°C for further analysis PET scans were analyzed with PMOD (version 3.8, PMOD Technologies). Volume of interests (VOIs) were drawn as spheres based on weight of organs found in the biodistribution. Data is expressed as mean standardized uptake value (SUV_{mean}). PET scans are visualized as a coronal projection containing the tumor or maximum intensity projections (MIP) scaled to 30% as maximal intensity.

***Ex-vivo* Tissue Analysis**

Formalin-fixed paraffin embedded (FFPE) tissues were sliced to 4 µm sections and mounted on tissue slides. For autoradiography, phosphor imaging screens (PerkinElmer) were exposed to the tissue slides in X-ray cassettes for 24-72 hours and digitized by the Cyclone Phosphor System (PerkinElmer). Autoradiography images were analyzed with ImageJ 1.52p (US NIH). Tissues were stained with hematoxylin and eosin (H&E) for tissue morphology. When possible, in subsequent 4 µm sections T-cell presence was visualized immunohistochemically (IHC) for mouse CD3 with a rabbit anti-mouse CD3 antibody, clone: SP7 (Abcam; ab16669). EpCAM presence was confirmed by a rabbit anti-mouse EpCAM antibody (Abcam; ab71916). For both stainings, antigen retrieval was 15 minutes at 95°C in citrate buffer at pH 6. For CD3 staining the primary antibody dilution was 1:50, for the EpCAM staining a 1:250 dilution was used. Next, a peroxidase

conjugated goat anti-rabbit antibody (Dako; p0448) was used, 1:100 dilution. For EpCAM staining a tertiary antibody was used, a peroxidase conjugated rabbit anti-goat antibody with 1:100 dilution (Dako; p0449). 3-3'-diaminobenzidine (DAB) was added to visualize peroxidase activity. For CD3 and EpCAM IHC, any membrane staining was considered positive. Slides were viewed with NDP.view2 (Hamamatsu).

Lysates of tumor, liver and spleen were prepared using RIPA buffer (ThermoFischer Scientific) including 1% protease blocker (ThermoFischer Scientific) and 1% phosphatase blocker (ThermoFischer Scientific). Together with plasma and intact [^{89}Zr]Zr-DFO-*N*-suc-muS110, they were loaded into mini-PROTEAN TGX precast gels (Bio-Rad). Gel-exposed phosphor imaging screens were read out by the Cyclone Phosphor System to identify the molecular weight of the [^{89}Zr]Zr-DFO-*N*-suc-BiTE. Molecular weight of bands was identified using ProSieve color protein marker (Lonza).

Statistical Methods

Data is presented as median with interquartile range. A Bonferroni corrected Mann-Whitney U-test was performed to test differences between groups (GraphPad, Prism 7). *P* values ≤ 0.05 were considered statistically significant. Blood half-life was calculated using a two-phase decay (GraphPad, Prism 7).

RESULTS

Conjugation and Labeling of BiTE Molecules with ^{89}Zr

N-suc-DFO-BiTE molecules were labeled with ^{89}Zr with a radiochemical purity of >95% (Supplementary Fig. 1A). Immunoreactivity was maintained for muS110, targeting mouse CD3ε and murine EpCAM and hyS110, targeting mouse CD3ε and human EpCAM, after conjugation to *N*-suc-DFO (Supplementary Fig. 1B), despite the formation

of 10-14% aggregates for muS110 and hyS110 as revealed by SE-HPLC (Supplementary Fig. 1A). Moreover, conjugated muS110 maintained similar *in-vitro* cytotoxicity (Supplementary Fig. 1C) and T-cell activation (Supplementary Fig. 1D) compared to parental muS110.

[^{89}Zr]Zr-DFO-*N*-suc-muS110 PET-imaging over Time in 4T1-bearing Immunocompetent Mice

To evaluate the role of binding to EpCAM on distribution of the BiTE molecules, immunodeficient mice were used. Accumulation of signal over time was seen in the tumor, spleen and liver in the MIPs of PET scans of [^{89}Zr]Zr-DFO-*N*-suc-muS110. High tracer signal was observed in the kidneys and bladder, indicating renal clearance (Fig. 1A). [^{89}Zr]Zr-DFO-*N*-suc-muS110 tumor and liver uptake over time was confirmed by coronal PET images (Fig. 1A). Blood half-life, based on the SUV_{mean} of the heart, was 0.4 hours (distribution) and 12.8 hours (elimination) (Fig. 1B). Over time, uptake in spleen increased until 24 hours, SUV_{mean} = 1.7 (1.5 to 1.9), and uptake in the tumor increased until 6 hours post injection, SUV_{mean} = 1.0 (0.8 to 1.3; Fig. 1C). After 24 hours, tumor- and spleen-to-blood ratios of SUV_{means} were 2.7 (2.3 to 3.3) and 6.5 (5.8 to 7.5).

[^{89}Zr]Zr-DFO-*N*-suc-BiTE Molecules in 4T1-bearing Immunocompetent Mice

High kidney uptake was seen with the CD3-targeting BiTE molecules ^{89}Zr-muS110 and ^{89}Zr-hyS110 and control BiTE molecule [^{89}Zr]Zr-DFO-*N*-suc-AMG 110 in the MIPs 24 hours after tracer administration (Fig. 2A). Uptake in the spleen and liver for [^{89}Zr]Zr-DFO-*N*-suc-muS110 and [^{89}Zr]Zr-DFO-*N*-suc-hyS110 but not for control [^{89}Zr]Zr-DFO-*N*-suc-AMG 110 was visualized in the coronal projections (Fig. 2A).

Ex-vivo biodistribution confirmed that spleen uptake of [^{89}Zr]Zr-DFO-*N*-suc-muS110 was higher than of [^{89}Zr]Zr-DFO-*N*-suc-AMG 110 but no difference was observed between [^{89}Zr]Zr-DFO-*N*-suc-muS110 and [^{89}Zr]Zr-DFO-*N*-suc-hyS110 (Fig. 2B and Supplementary Table 1). Also in other lymphoid tissues, such as the mesenteric lymph nodes, uptake of [^{89}Zr]Zr-DFO-*N*-suc-muS110 and [^{89}Zr]Zr-DFO-*N*-suc-hyS110 was increased compared to aspecific uptake of [^{89}Zr]Zr-DFO-*N*-suc-AMG 110. Tumor uptake did not differ between [^{89}Zr]Zr-DFO-*N*-suc-muS110 and [^{89}Zr]Zr-DFO-*N*-suc-AMG 110 or [^{89}Zr]Zr-DFO-*N*-suc-hyS110. [^{89}Zr]Zr-DFO-*N*-suc-muS110 accumulated more in the duodenum than [^{89}Zr]Zr-DFO-*N*-suc-hyS110 and [^{89}Zr]Zr-DFO-*N*-suc-AMG 110.

SDS-PAGE autoradiography showed intact [^{89}Zr]Zr-DFO-*N*-suc-muS110 in the tumor lysates and plasma, while disintegrated tracer was found in the spleen and liver lysates (Supplementary Fig. 2).

[^{89}Zr]Zr-DFO-*N*-suc-BiTE Molecules in 4T1-bearing Immunodeficient Mice

PET scans showed no spleen uptake of [^{89}Zr]Zr-DFO-*N*-suc-muS110 or [^{89}Zr]Zr-DFO-*N*-suc-AMG 110 in immunodeficient mice (Fig. 3A). For [^{89}Zr]Zr-DFO-*N*-suc-muS110 MIPs showed, apart from the high uptake in the kidneys, little uptake in other organs.

Similar tumor uptake of [^{89}Zr]Zr-DFO-*N*-suc-muS110 and [^{89}Zr]Zr-DFO-*N*-suc-AMG 110 was confirmed by e*x-vivo* biodistribution in these immunodeficient mice (Fig. 3B and Supplementary Table 2). No differences in uptake in spleen and mesenteric lymph nodes were found. Uptake of [^{89}Zr]Zr-DFO-*N*-suc-muS110 was higher than of [^{89}Zr]Zr-DFO-*N*-suc-AMG 110 in high-EpCAM expressing tissues like the pancreas, duodenum, and ileum.

[^{89}Zr]Zr-DFO-*N*-suc-BiTE Molecules in 4T1-bearing Immunocompetent Mice after Repeated MuS110 Administration

Ex-vivo biodistribution of immunocompetent mice that received 10 µg muS110 iv daily for 5 days showed lower tumor uptake of [^{89}Zr]Zr-DFO-*N*-suc-muS110 than [^{89}Zr]Zr-DFO-*N*-suc-AMG 110 and higher spleen uptake of [^{89}Zr]Zr-DFO-*N*-suc-muS110 (Fig. 4A and Supplementary Table 3).

The comparison of ^{89}Zr-muS110 biodistribution in the three different settings, immunocompetent, immunodeficient, and repeated administration group, revealed lower uptake in the immunodeficient and the repeated administration setting in the lymphoid tissues such as spleen and mesenteric lymph nodes (Fig. 4B and Supplementary Table 4). Biodistribution of control [^{89}Zr]Zr-DFO-*N*-suc-AMG 110 in the three settings was comparable (Supplementary Fig. 3 and Supplementary Table 5).

Additionally, in the immunocompetent model uptake of [^{89}Zr]Zr-DFO-*N*-suc-muS110 is higher in the digestive tract and the tumor compared to the other models (Fig. 4B), indicating specific uptake in the immunocompetent model and target saturation after repeated administration of muS110.

Microscopic Analysis of Tissues *Ex-vivo* to Determine the Cellular Source of BiTE Molecule Uptake

Autoradiography showed heterogenous tumor uptake in immunocompetent mice (Fig. 5). High local uptake in the tumor colocalized with high expression of CD3 for [^{89}Zr]Zr-DFO-*N*-suc-muS110 and [^{89}Zr]Zr-DFO-*N*-suc-hyS110, while this was not seen for [^{89}Zr]Zr-DFO-*N*-suc-AMG 110. Furthermore, no difference in EpCAM expression was observed between higher and lower uptake areas in the tumor. In the spleen, areas of

high uptake of [^{89}Zr]Zr-DFO-*N*-suc-muS110 and [^{89}Zr]Zr-DFO-*N*-suc-hyS110 colocalized with white pulp, where high numbers of T-cells were found immunohistochemically (Supplementary Fig. 4). Although IHC-staining for EpCAM in spleen tissue can show non-specific staining (*14*), we see increased staining in the red pulp where autoradiography detected less uptake of [^{89}Zr]Zr-DFO-*N*-suc-muS110 and [^{89}Zr]Zr-DFO-*N*-suc-hyS110.

Higher uptake in the duodenum of the immunocompetent mice of [^{89}Zr]Zr-DFO-*N*-suc-muS110 and [^{89}Zr]Zr-DFO-*N*-suc-hyS110 versus [^{89}Zr]Zr-DFO-*N*-suc-AMG 110 observed in the biodistribution (Fig. 2B) was confirmed by autoradiography (Supplementary Fig. 5A). The uptake in the duodenum was homogenous. Immunohistochemical staining confirmed a homogenous presence of both CD3-positive T-cells and EpCAM-positive cells in the duodenum (Supplementary Fig 5B).

DISCUSSION

This study in immunocompetent mice shows that the [^{89}Zr]Zr-DFO-*N*-suc-muS110 distribution is predominantly mediated by its higher affinity for CD3 compared to EpCAM. This results in specific uptake in tissues with high numbers of CD3-positive T-cells, such as the spleen, mesenteric lymph nodes and duodenum. In our immunocompetent mouse model CD3-targeting BiTE molecule [^{89}Zr]Zr-DFO-*N*-suc-hyS110 behaved similarly to [^{89}Zr]Zr-DFO-*N*-suc-muS110, despite [^{89}Zr]Zr-DFO-*N*-suc-muS110 having an additional EpCAM-targeting arm. This demonstrates the limited influence of the EpCAM targeting arm for this BiTE molecule. In contrast to the immunocompetent model, in our immunodeficient mouse model no difference in uptake in lymphoid tissues for [^{89}Zr]Zr-DFO-*N*-suc-muS110 and [^{89}Zr]Zr-DFO-*N*-suc-AMG 110 was seen.

This paper therefore adds novel insight into the distribution of BiTE molecules by using an immunocompetent mouse model and murine BiTE molecules. Previously, preclinically ^{89}Zr-labeled BiTE molecules failed to show uptake in lymphoid organs as human BiTE molecules were tested in immunodeficient mouse models (*10,11*). Recently, apart from uptake in tumor lesions, clear uptake was shown for the CEA/CD3 BiTE molecule ^{89}Zr-labeled AMG 211 in the spleen in patients with advanced gastrointestinal adenocarcinomas (*12*). For AMG 211, the affinity for CEA was higher (K_D = 5.5 nM) than for CD3 (K_D = 310 nM). In transgenic mice expressing human CD3, a bispecific antibody targeting CD3 and HER2 with the same affinity for both antigens (K_D = 0.5 nM) showed high accumulation in lymphoid tissues in contrast to the same bispecific antibody with lower affinity for CD3 (K_D = 50 nM). Parallel to the accumulation in the lymphoid tissues of the high CD3 affinity bispecific antibody, there was reduced uptake in the tumor (*18*). Our findings contribute to the growing understanding that the interplay between binding arms of a bispecific antibody is complex and that especially the affinity for the immune component will greatly influence its biodistribution.

In cynomolgus monkeys, systemic cytokine release, indicative for immune-related adverse effects, depended on the affinity of the CD3 arm of a bispecific antibody targeting CD3 and CLL-1 (*19*). In transgenic mice, a high affinity CD3-binding arm directed bispecific antibodies to lymphoid tissues (*18*), thus providing additional rational for molecular imaging in immunocompetent mouse models to assess lymphoid uptake when translating bispecific antibodies.

A limited role for the tumor-targeting arm directed against EpCAM of [^{89}Zr]Zr-DFO-*N*-suc-muS110 was found in this paper. This can be explained by the lower affinity for

EpCAM than for CD3 (K_D = 21 vs 2.9 nM). However, in the absence of T-cells in the immunodeficient model little specific uptake was observed in high-EpCAM expressing tissues. [^{89}Zr]Zr-DFO-*N*-suc-muS110 did accumulate more in the high-EpCAM expressing tissues pancreas and duodenum than [^{89}Zr]Zr-DFO-*N*-suc-AMG 110, but uptake was still lower compared to the uptake in these tissues of [^{89}Zr]Zr-DFO-*N*-suc-muS110 in the immunocompetent group. Higher EpCAM-mediated uptake in the immunodeficient model may been expected, due to the elimination of competition for CD3. In a human EpCAM expressing transgenic mouse model where the biodistribution of iodine-125 labeled anti-EpCAM antibodies was quantified, equal low tumor uptake was observed in an EpCAM-positive and EpCAM-negative tumor. High uptake in healthy EpCAM-expressing tissue was observed, such as the pancreas and ileum (*20*). EpCAM being expressed by numerous healthy tissues can serve as a sink and limit the availability of the anti-EpCAM antibody for the tumor. This can also be an explanation for the lacking evidence for EpCAM-specific tumor uptake of [^{89}Zr]Zr-DFO-*N*-suc-muS110 compared to the ^{89}Zr-AMG 110 tumor uptake in an immunodeficient mouse model bearing a human EpCAM-positive tumor (*10*).

Fast renal clearance and splenic uptake of ^{89}Zr-muS110 might have also prevented tumor uptake. Higher doses could not be explored due to the low maximum tolerable dose of muS110 in mice (*17*). However, after repeated administration of muS110 a reduction in uptake of [^{89}Zr]Zr-DFO-*N*-suc-muS110 in various tissues was noticed, indicative of target saturation. T-cells in the circulation can redistribute after a single bolus injection of muS110 and return to base levels, meanwhile splenic CD8+ T-cell levels are unaffected (*17*). Target saturation seems in line with the clinical ^{89}Zr-AMG 211 PET-

imaging. Here, ^{89}Zr-AMG 211 imaging was performed in two patients at the end of the second 28-days continuous IV treatment with AMG 211. A ~2-3-fold higher presence in the blood pool and a ~2-3-fold lower kidney uptake but absence of tumor tracer uptake were seen in patients during BiTE treatment. The absence of tumor visualization is likely indicative of tumor target saturation (*12*).

In the tumor from the immunocompetent mouse group uptake of [^{89}Zr]Zr-DFO-*N*-suc-muS110 and [^{89}Zr]Zr-DFO-*N*-suc-hyS110 was seen in areas with T-cells. This proves that the tumors are accessible and uptake is mainly driven by CD3. Nevertheless, [^{89}Zr]Zr-DFO-*N*-suc-muS110 did not accumulate more in the tumor than control ^{89}Zr-AMG 110 in either the immunocompetent and the immunodeficient group. However, daily administration of muS110 led to a reduction in tumor uptake of [^{89}Zr]Zr-DFO-*N*-suc-muS110, indicating that the tumor uptake in the immunocompetent mouse model is specific. Competition for [^{89}Zr]Zr-DFO-*N*-suc-muS110 between the CD3-rich tissues, leading to its distribution to lymphoid tissues, could be an explanation for a similar accumulation of [^{89}Zr]Zr-DFO-*N*-suc-muS110 and [^{89}Zr]Zr-DFO-*N*-suc-AMG 110 in the tumor of the immunocompetent mice. Accumulation of [^{89}Zr]Zr-DFO-*N*-suc-AMG 110 in the tumor will be non-specific, and therefore not hindered by any competition. Testing a range of affinities for both the CD3 and the EpCAM targeting arm of muS110 would show if we can shift the distribution away from the lymphoid tissues. However, such BiTE molecules were not developed.

In conclusion, the distribution of [^{89}Zr]Zr-DFO-*N*-suc-muS110 is predominantly mediated by its affinity for CD3. This results in uptake in tissues with high numbers of T-cells, including immune-infiltrated tumors. A role for the arm targeting the tumor-

associated antigen, here in this specific example EpCAM, was absent in the biodistribution of [^{89}Zr]Zr-DFO-*N*-suc-muS110. These findings highlight the need for extensive biodistribution studies of novel bispecific constructs to support their specific drug development and determine their potential for clinical translation. Attention should be paid to the affinity of the CD3-targeting arm to prevent uptake in the lymphoid tissues and associated undesired effects.

ACKNOWLEDGEMENTS

The authors thank Linda Pot-de Jong and Laura von Iven for immunohistochemical staining.

Key points

Question: What is the influence of the T-cell targeting arm (CD3) and the tumor targeting arm (EpCAM) of this bispecific T-cell engager (BiTE) molecule (CD3/EpCAM) on the whole-body biodistribution in mice?

Pertinent findings: This comparison biodistribution study with different zirconium-89 (^{89}Zr) labeled mouse BiTE molecules in immunocompetent and immunodeficient mouse models revealed that the biodistribution of the BiTE molecule muS110 (CD3/EpCAM) is mainly dependent on the T-cell targeting arm with limited contribution of its tumor-targeting arm, targeting EpCAM.

Implications for patient care: Extensive biodistribution studies of novel bispecific constructs are needed where extra attention should be paid to the affinity of the CD3-

targeting arm in an effort to prevent uptake in the lymphoid tissues and associated undesired effects.

REFERENCES

1. Carter PJ, Lazar GA. Next generation antibody drugs: pursuit of the 'high-hanging fruit'. *Nat Rev Drug Discov*. 2018;17:197–223.
2. Mack M, Riethmuller G, Kufer P. A small bispecific antibody construct expressed as a functional single-chain molecule with high tumor cell cytotoxicity. *Proc Natl Acad Sci USA*. 1995;92:7021–7025.
3. Offner S, Hofmeister R, Romaniuk A, Kufer P, Baeuerle PA. Induction of regular cytolytic T cell synapses by bispecific single-chain antibody constructs on MHC class I-negative tumor cells. *Mol Immunol*. 2006;43:763–771.
4. Haas C, Krinner E, Brischwein K, et al. Mode of cytotoxic action of T cell-engaging BiTE antibody MT110. *Immunobiology*. 2009;214:441–453.
5. Brischwein K, Parr L, Pflanz S, et al. Strictly target cell-dependent activation of T cells by bispecific single-chain antibody constructs of the BiTE class. *J Immunother*. 2007;30:798–807.
6. Ravandi F, Stein AS, Kantarjian HM, et al. A phase 1 first-in-human study of AMG330, an anti-CD33 bispecific T-cell engager (BiTE®) antibody construct, in relapsed/refractory acute myeloid leukemia (R/R AML). *Blood*. 2018;132 (Suppl 1):25.
7. Klinger M, Benjamin J, Kischel R, Stienen S, Zugmaier G. Harnessing T cells to fight cancer with BiTE(®) antibody constructs - past developments and future directions. *Immunol Rev*. 2016;270:193–208.
8. Labrijn AF, Janmaat ML, Reicher JM, Parren PWHI. Bispecific antibodies: a mechanisctic review of the pipeline. *Nature Rev Drug Discov*. 2019;18: 585–608

9. Suurs FV, Lub-de-Hooge MN, de Vries EGE, de Groot DJ. A review of bispecific antibodies and antibody constructs in oncology and clinical challenges. *Pharmacol Ther*. 2019;201:103-119
10. Warnders FJ, Waaijer SJH, Pool M, et al. Biodistribution and PET imaging of labeled bispecific T cell-engaging antibody targeting EpCAM. *J Nucl Med*. 2016;57:812–817.
11. Waaijer SJH, Warnders FJ, Stienen S, et al. Molecular imaging of radiolabeled bispecific T-cell engager ^{89}Zr-AMG211 targeting CEA-positive tumors. *Clin Cancer Res*. 2018;24:4988–96.
12. Moek KL, Waaijer SJH, Kok IC, et al. ^{89}Zr-labeled bispecific T-cell engager AMG 211 PET shows AMG 211 accumulation in CD3-rich tissues and clear, heterogeneous tumor uptake. *Clin Cancer Res*. 2019;25:3517-3527.
13. Went PT, Lugli A, Meier S, et al. Frequent EpCam protein expression in human carcinomas. *Hum Pathol*. 2004;35:122–128.
14. Amann M, Brischwein K, Lutterbuese P, et al. Therapeutic window of MuS110, a single-chain antibody construct bispecific for murine EpCAM and murine CD3. *Cancer Res*. 2008;68:143–151.
15. Brischwein K, Schlereth B, Guller B, et al. MT110: a novel bispecific single-chain antibody construct with high efficacy in eradicating established tumors. *Mol Immunol*. 2006;43:1129–1143.
16. Verel I, Visser GWM, Boellaard R, Stigter-van Walsum M, Snow GB, van Dongen GAMS. ^{89}Zr immuno-PET: comprehensive procedures for the production of ^{89}Zr-labeled monoclonal antibodies. *J Nucl Med*. 2003;44:1271–1281.

17. Amann M, Friedrich M, Lutterbuese P, et al. Therapeutic window of an EpCAM/CD3-specific BiTE antibody in mice is determined by a subpopulation of EpCAM-expressing lymphocytes that is absent in humans. *Cancer Immunol Immunother*. 2009;58:95–109.
18. Mandikian D, Takahashi N, Lo AA, et al. Relative target affinities of T-cell-dependent bispecific antibodies determine biodistribution in a solid tumor mouse model. *Mol Cancer Ther*. 2018;17:776–785.
19. Leong SR, Sukumaran S, Hristopoulos M, et al. An anti-CD3/anti-CLL-1 bispecific antibody for the treatment of acute myeloid leukemia. *Blood*. 2017;129:609–618.
20. Kosterink JGW, McLaughlin PMJ, Lub-de Hooge MN, et al. Biodistribution studies of epithelial cell adhesion molecule (EpCAM)-directed monoclonal antibodies in the EpCAM-transgenic mouse tumor model. *J immunol*. 2007; 179:1362–1368.

Figures

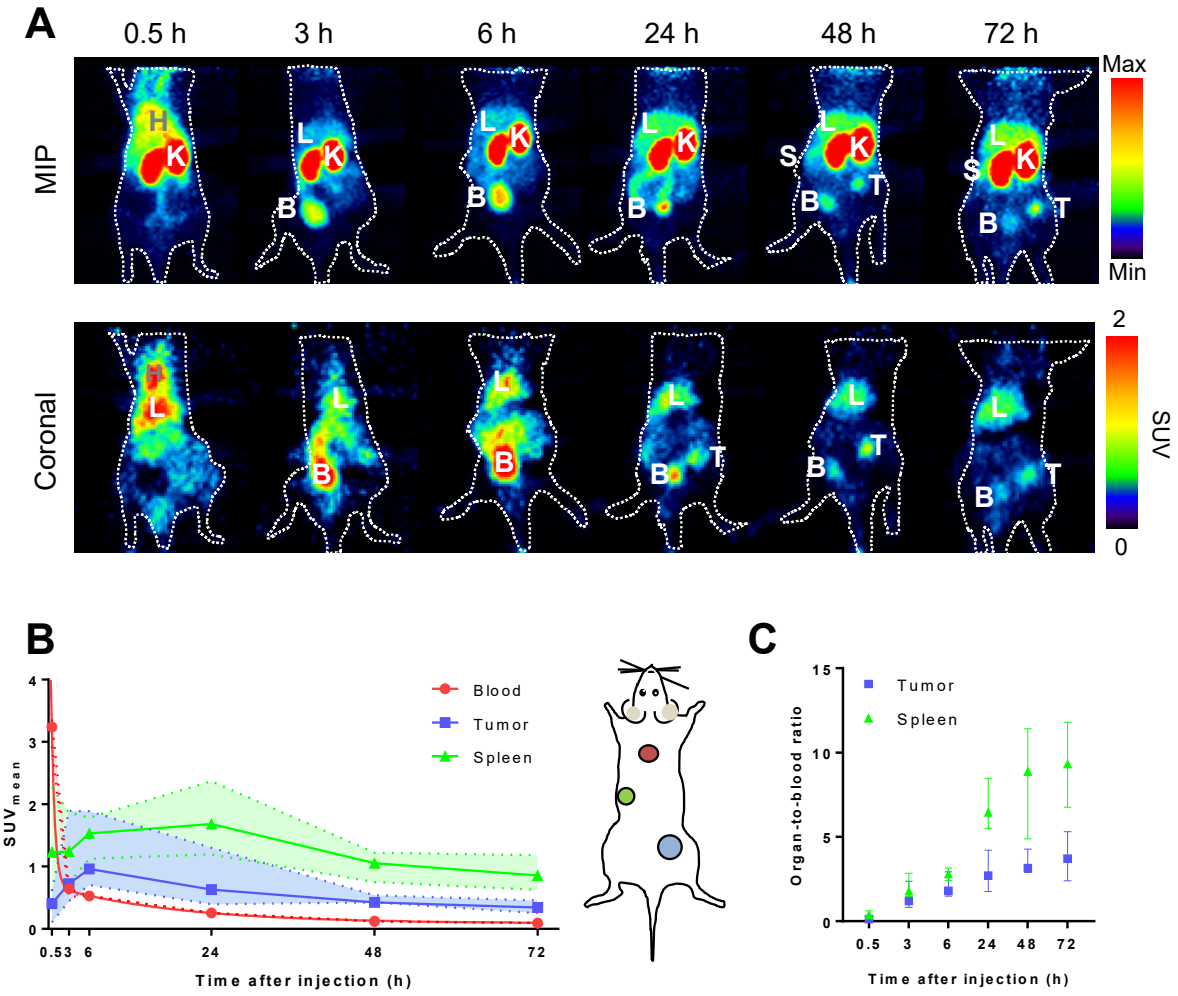

Figure 1. PET biodistribution of 10 µg [^{89}Zr]Zr-DFO-*N*-suc-muS110 in 4T1-tumor immunocompetent mice (*n* = 6). **A,** Representative serial coronal and maximum intensity projection PET images up to 72 hours after injection. L = liver; T = tumor; S = spleen; K = kidney; B = bladder; H = heart. **B,** Image quantification of blood, tumor and spleen. **C,** Image quantifications expressed as organ-to-blood ratio for tumor and spleen. Data is presented as median with interquartile range.

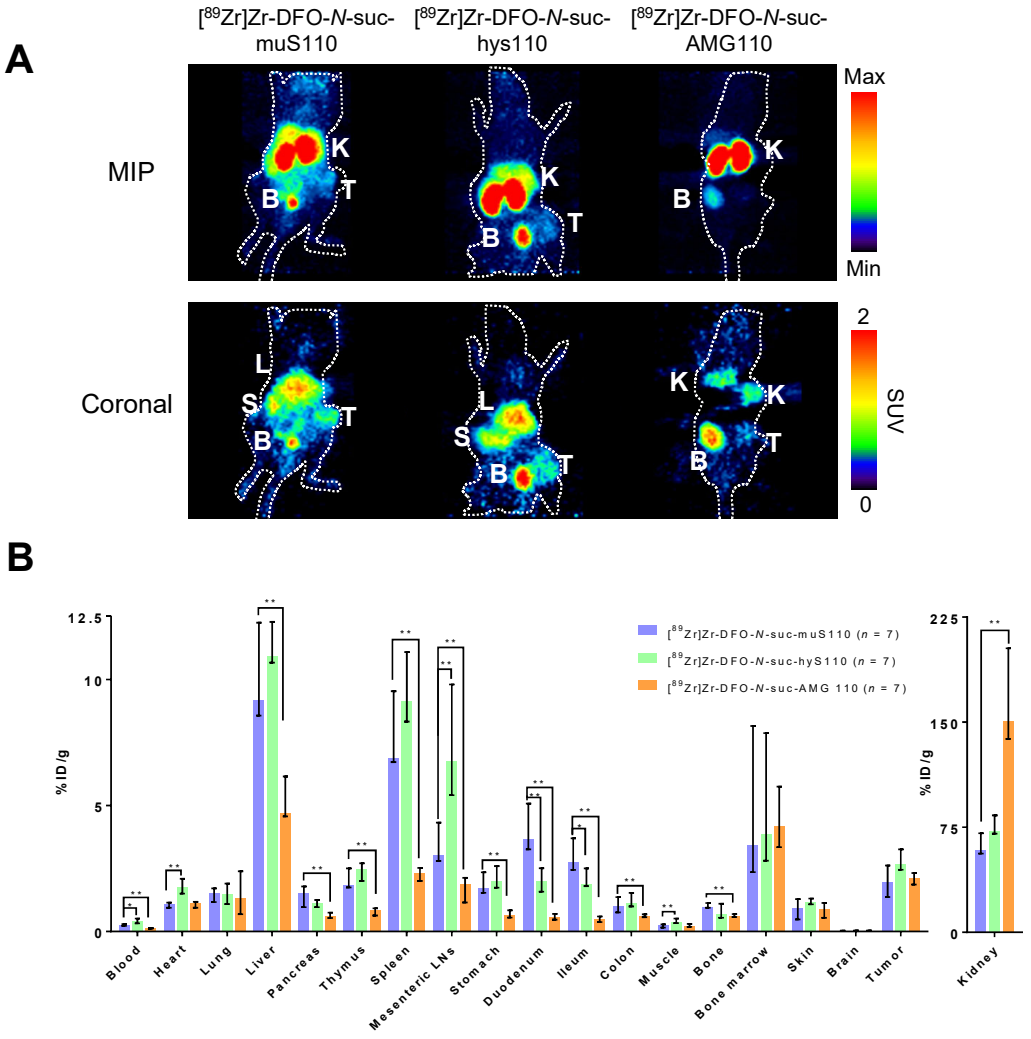

Figure 2. Biodistribution of 10 µg [^{89}Zr]Zr-DFO-*N*-suc-muS110 , [^{89}Zr]Zr-DFO-*N*-suc-hyS110 or [^{89}Zr]Zr-DFO-*N*-suc-AMG 110 (all $n = 7$) in 4T1-tumor bearing immunocompetent mice 24 hours pi. **A,** Coronal and maximum intensity projections of representative PET images 24 hours after injection of [^{89}Zr]Zr-DFO-*N*-suc-BiTE molecules. L = liver; T = tumor; S = spleen; K = kidney; B = bladder. **B,** *Ex-vivo* biodistribution, data is presented as median with interquartile range; *: $P \leq 0.05$, **: $P \leq 0.01$.

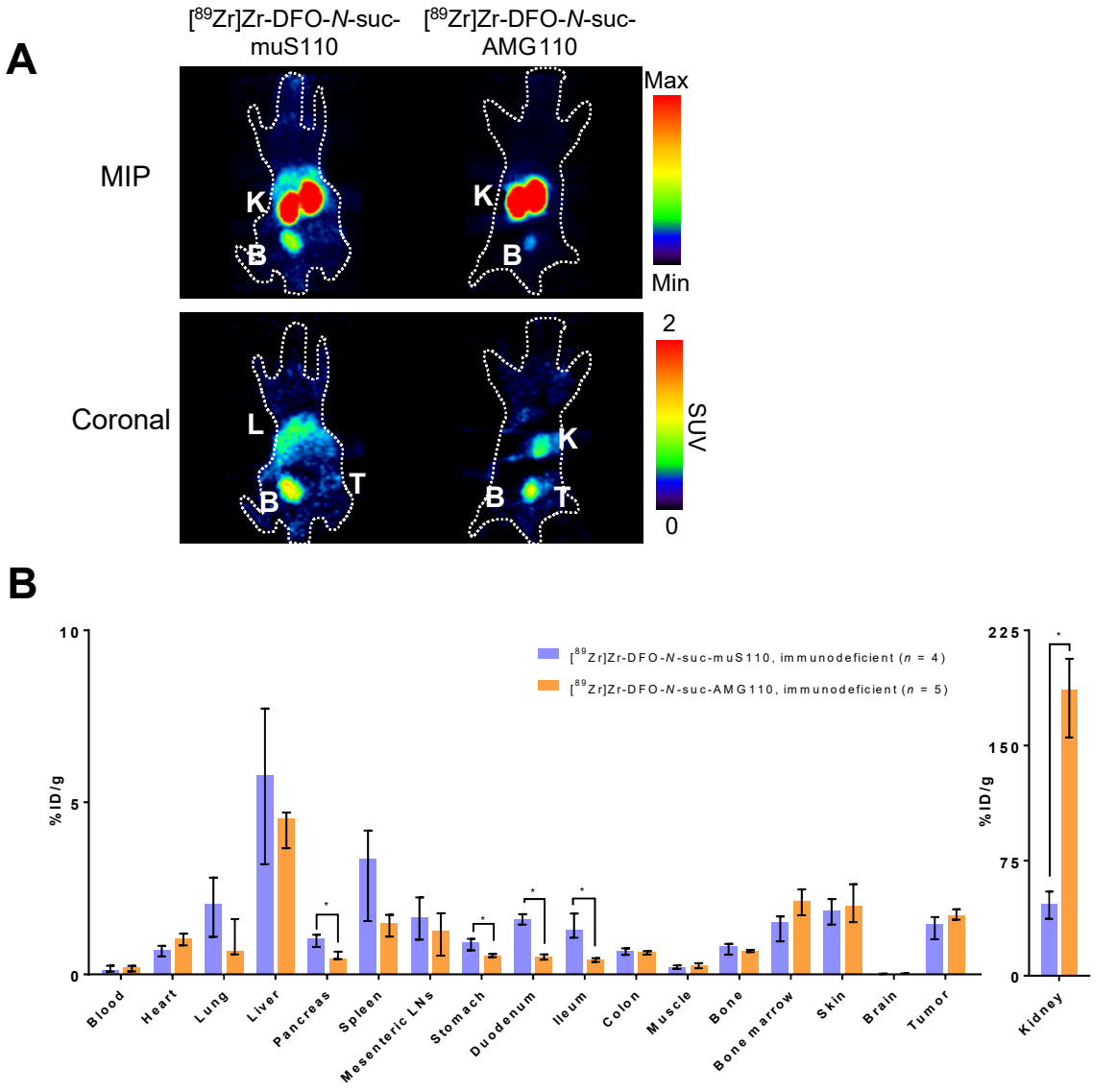

Figure 3. Biodistribution of 10 µg [^{89}Zr]Zr-DFO-*N*-suc-muS110 (*n* = 4) or [^{89}Zr]Zr-DFO-*N*-suc-AMG 110 (*n* = 5) in 4T1-tumor bearing immunodeficient mice 24 hours pi. **A,** Coronal and maximum intensity projections of representative PET images 24 hours after injection. L = liver; T = tumor; K = kidney; B = bladder. **B,** *Ex-vivo* biodistribution, data is presented as median with interquartile range; *: $P \leq 0.05$.

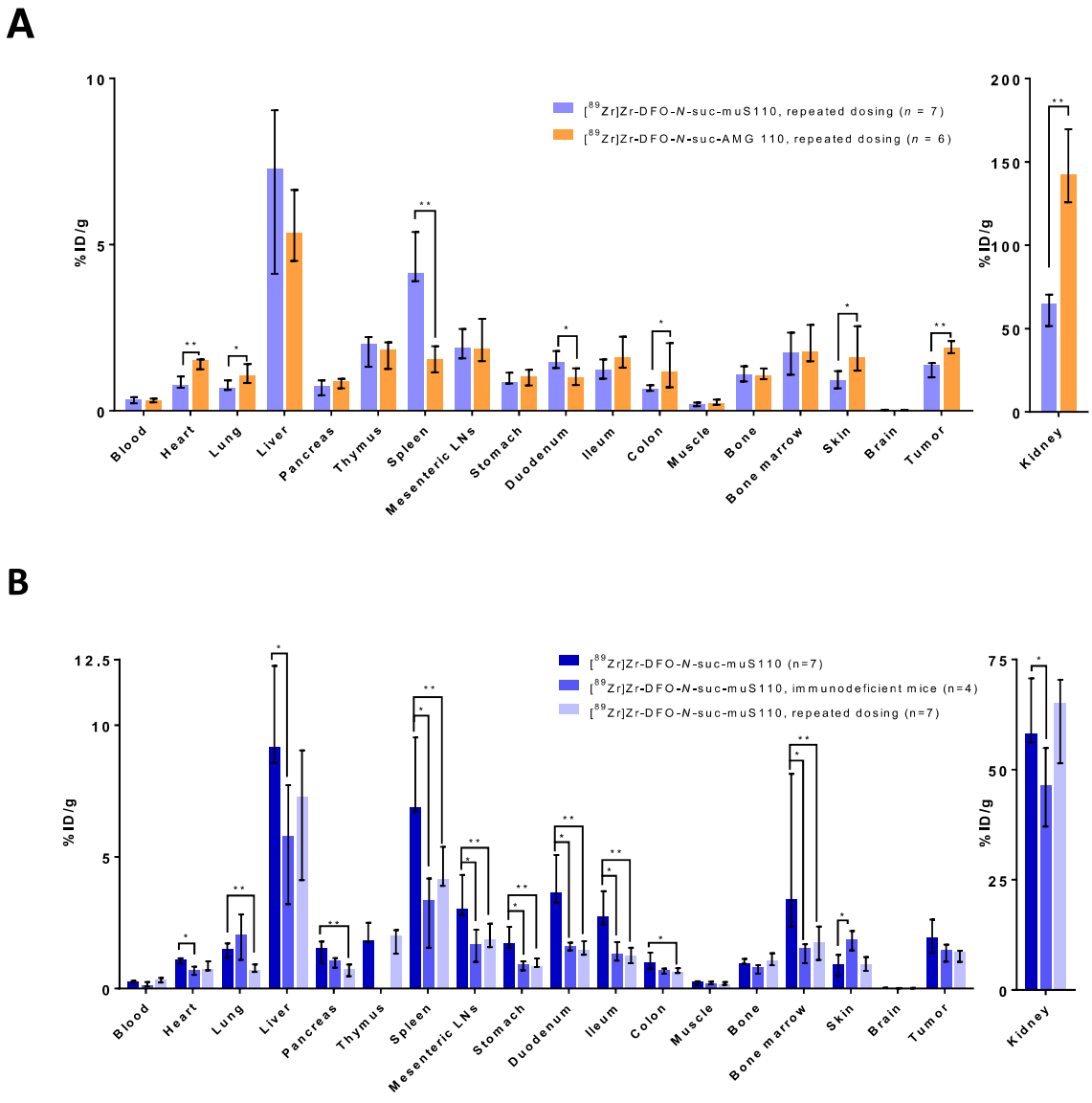

Figure 4. A, *Ex-vivo* biodistribution 24 hours after injection 10 µg [^{89}Zr]Zr-DFO-*N*-suc-muS110 (*n* = 7) or [^{89}Zr]Zr-DFO-*N*-suc-AMG110 (*n* = 6) in 4T1-tumor bearing immunocompetent mice after receiving 10 µg muS110 for 5 days. **B,** Comparing *ex-vivo* biodistribution of 10 µg [^{89}Zr]Zr-DFO-*N*-suc-muS110 to immunocompetent mice (*n* = 7), immunodeficient mice (*n* = 4) and repeated mus110 administration mice (*n* = 7), 24 hours pi. Data is presented as median with interquartile range; *: $P \leq 0.05$, **: $P \leq 0.01$.

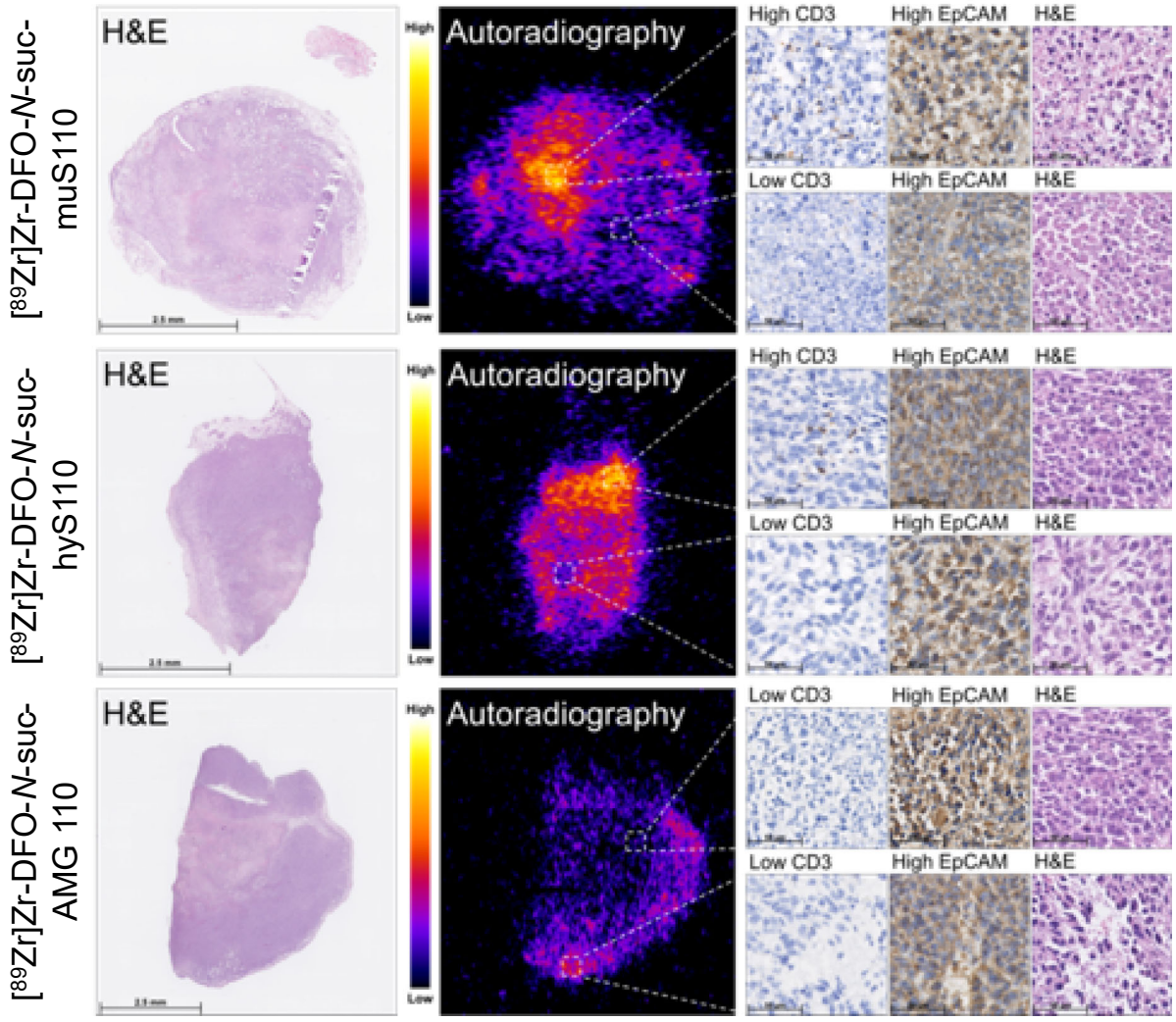

Figure 5. *Ex-vivo* microscopic analysis of 4T1-tumor tissue from immunocompetent mice 24 hours after injection of 10 µg [^{89}Zr]Zr-DFO-*N*-suc-BiTE molecule. From left to right, H&E staining and corresponding autoradiography, followed by CD3 and EpCAM IHC and H&E.

Supplementary data.

Biodistribution of a CD3/EpCAM bispecific T-cell engager is driven by the CD3 arm

Frans V. Suurs[1], Grit Lorenczewski[2], Sabine Stienen[2], Matthias Friedrich[2], Elisabeth G.E. de Vries[1], Derk Jan A. de Groot[1] and Marjolijn N. Lub-de Hooge[3].

[1]Department of Medical Oncology, University Medical Center Groningen, Groningen, the Netherlands; [2]Amgen Research Munich GmbH, Munich, Germany; [3]Department of Clinical Pharmacy and Pharmacology, University Medical Center Groningen, Groningen, the Netherlands;

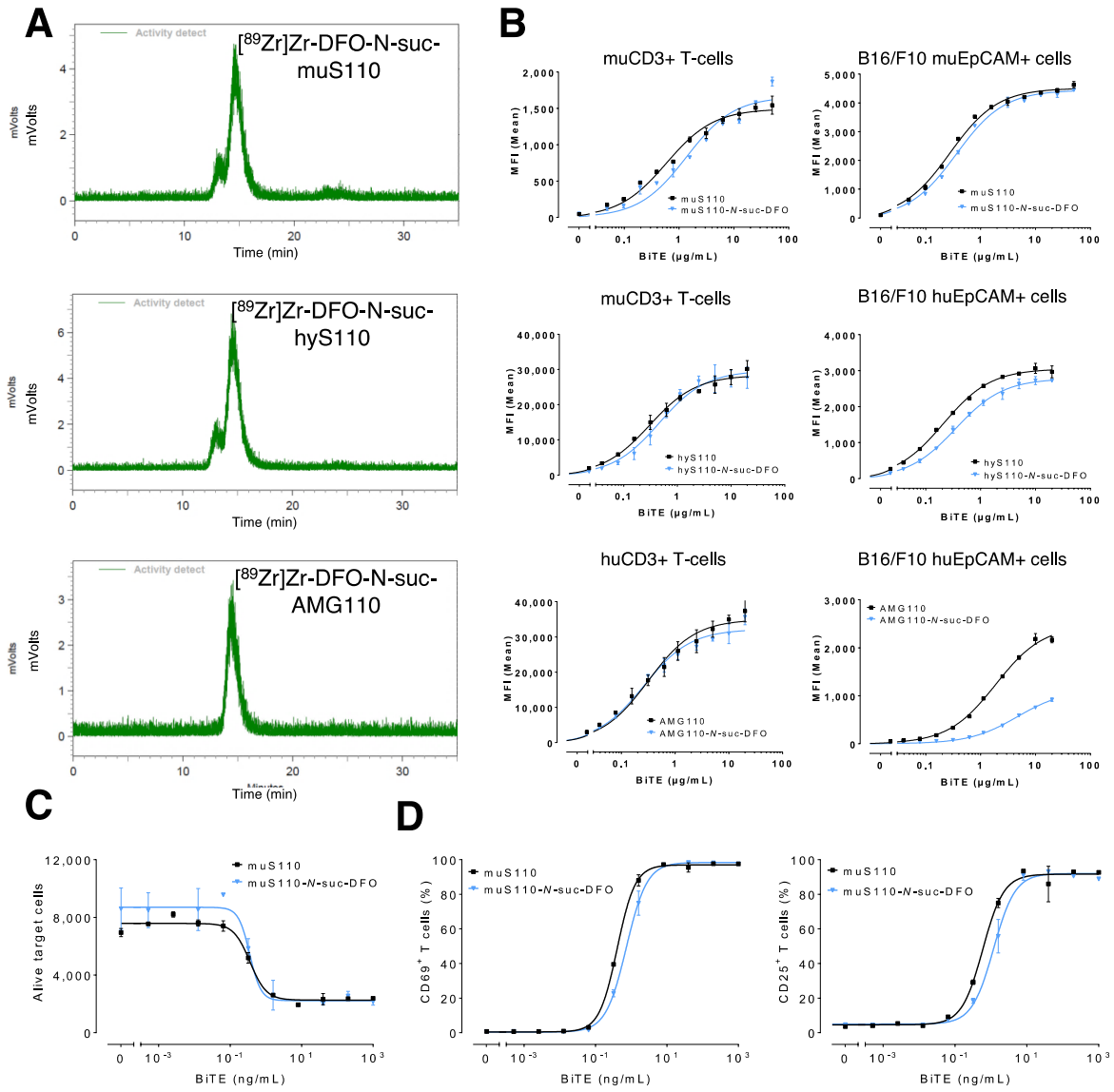

Supplementary figure 1. Evaluation and quality control and validation of [^{89}Zr]Zr-DFO-*N*-suc-BiTE molecules. **A**, Radiochemical signal of size exclusion high performance liquid chromatography chromatogram of [^{89}Zr]Zr-DFO-*N*-suc-BiTE antibody molecules. BiTE elutes after 15 minutes. Free ^{89}Zr elutes after 24 minutes. **B**, Binding of DFO-N-suc-BiTE antibody molecules tested on murine CD3-positive T-cells and B16/F10 murine EpCAM-positive cells. Functionality assessed by cell-based assays with T-cells: Tumor

cells incubated at a ratio of 10:1**.** The read-outs are cytotoxicity (**C**) and T-cell activation by CD69 and CD25 expression (**D**). Data are mean ± SD (*n* = 2).

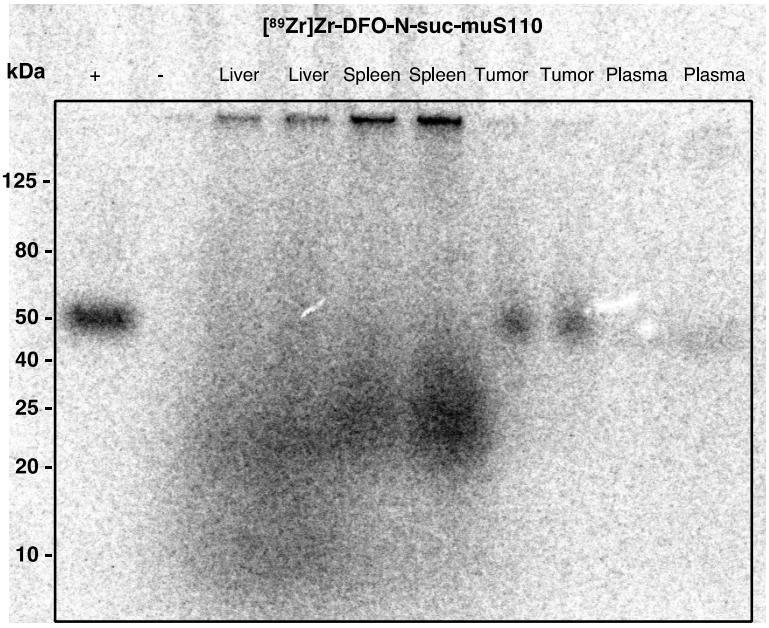

Supplementary figure 2. Integrity of 10 µg [^{89}Zr]Zr-DFO-*N*-suc-muS110 in 4T1-tumor bearing immunocompetent mice, 24 hours pi, by SDS-PAGE autoradiography. Lysates of liver spleen and tumor were loaded, as well as plasma of corresponding mice. + = [^{89}Zr]Zr-DFO-*N*-suc-muS110, - = empty lane.

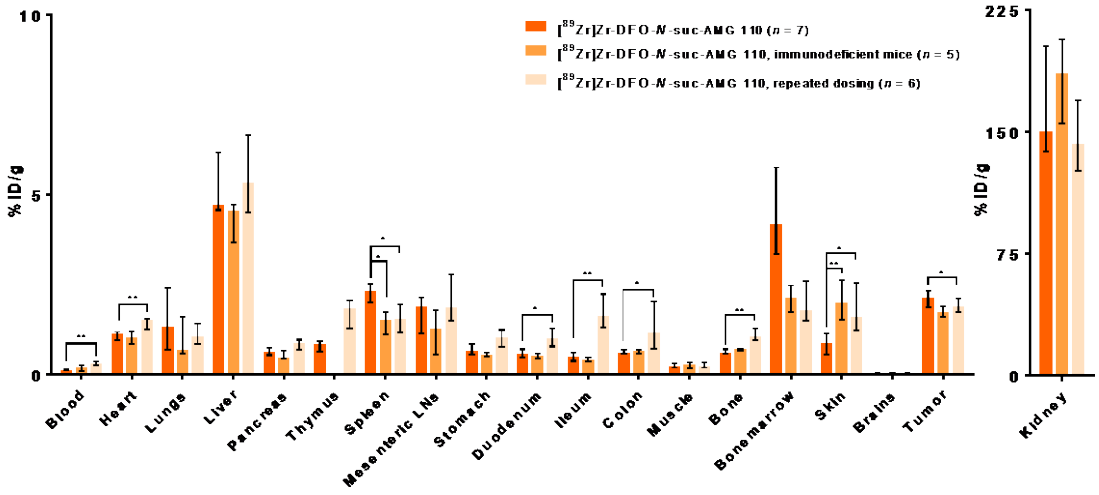

Supplementary figure 3. *Ex-vivo* biodistribution 24 hours after injection of 10 µg [^{89}Zr]Zr-DFO-*N*-suc-AMG 110 of immunocompetent mice (*n* = 7), immunodeficient mice (*n* = 5) and repeated mus110 administration mice (*n* = 6), 24 hours pi. Data is presented as median with interquartile range; *: $P \leq 0.05$, **: $P \leq 0.01$.

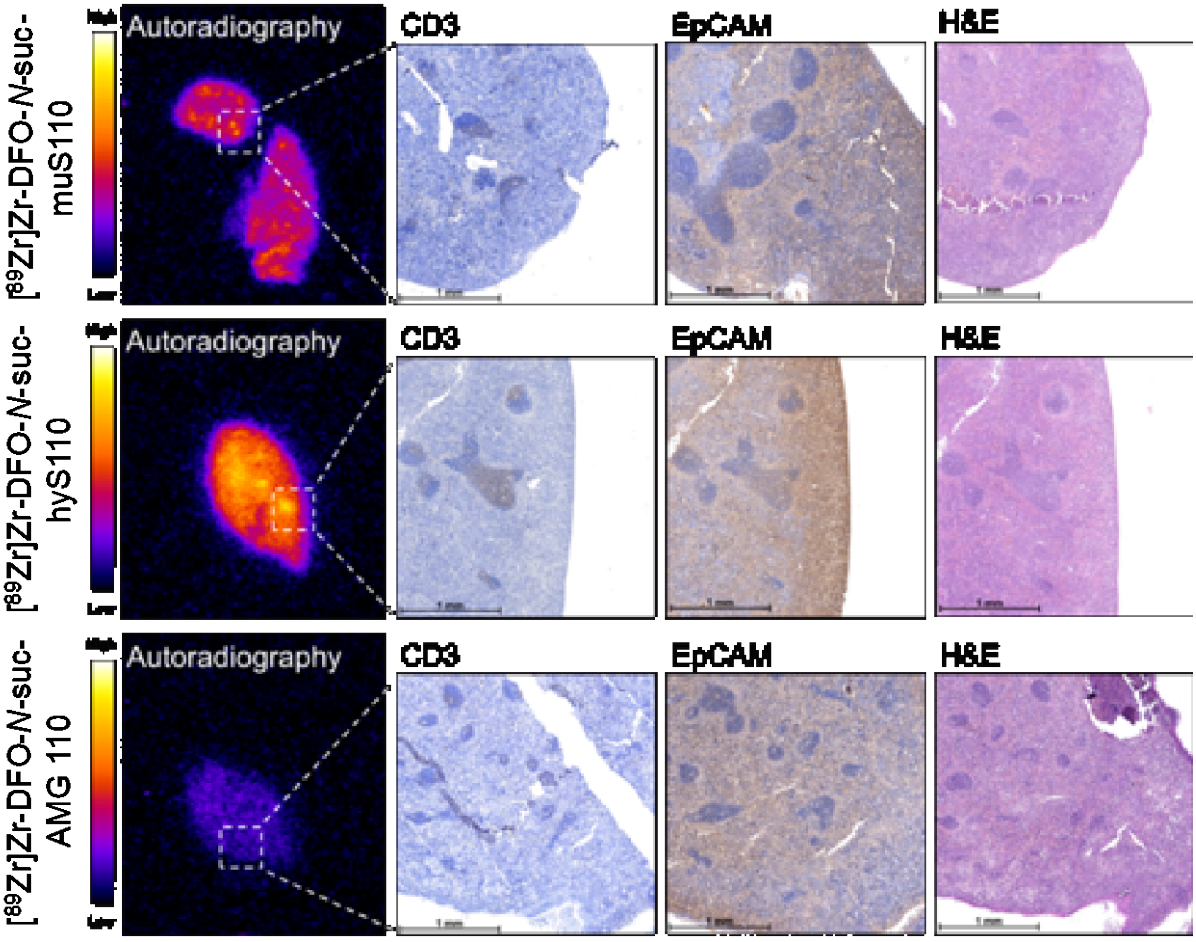

Supplementary figure 4. Microscopic analysis of the spleen from immunocompetent mice 24 hours after injection of 10 µg , [^{89}Zr]Zr-DFO-*N*-suc-BiTE molecule. From left to right, autoradiography followed by zoomed in CD3 and EpCAM IHC and H&E. From top to bottom, [^{89}Zr]Zr-DFO-*N*-suc-muS110, [^{89}Zr]Zr-DFO-*N*-suc-hyS110 and [^{89}Zr]Zr-DFO-*N*-suc-AMG 110.

A

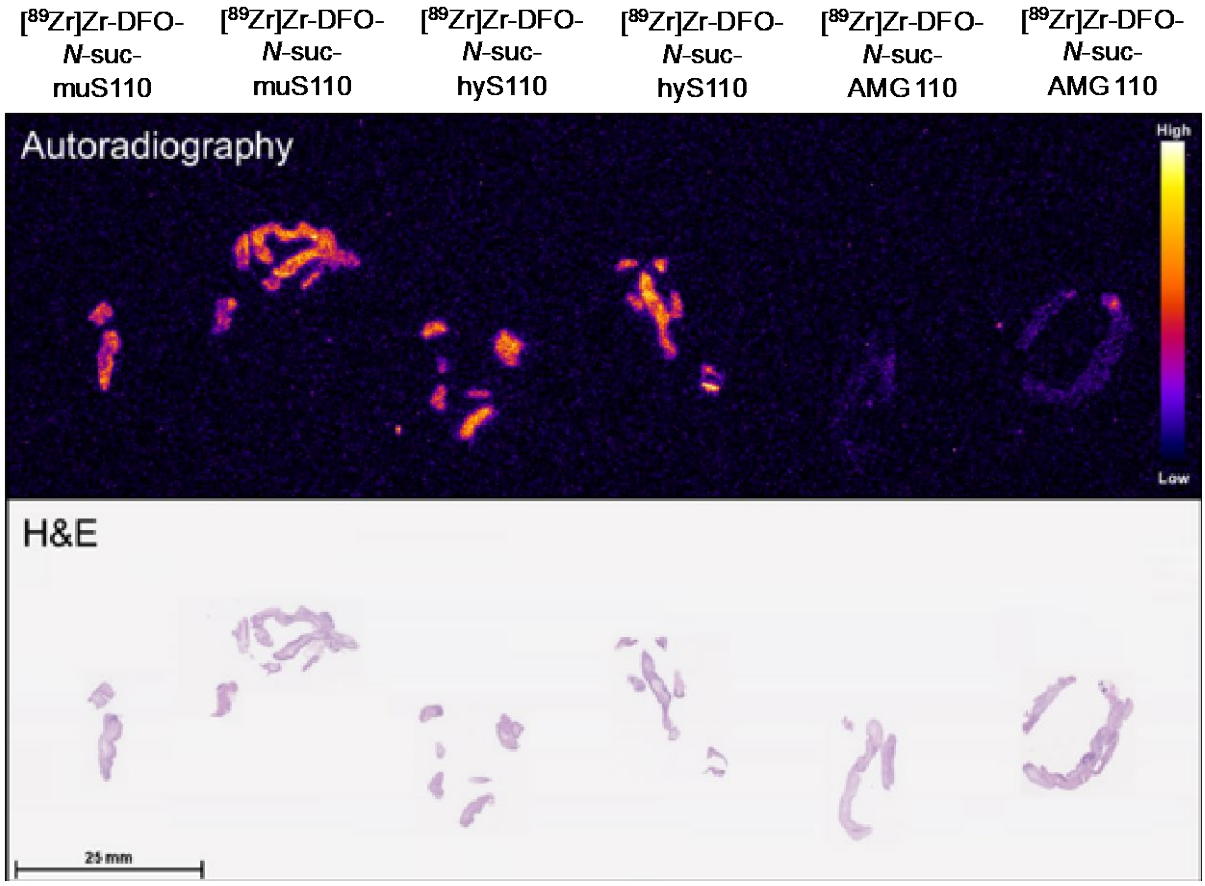

B

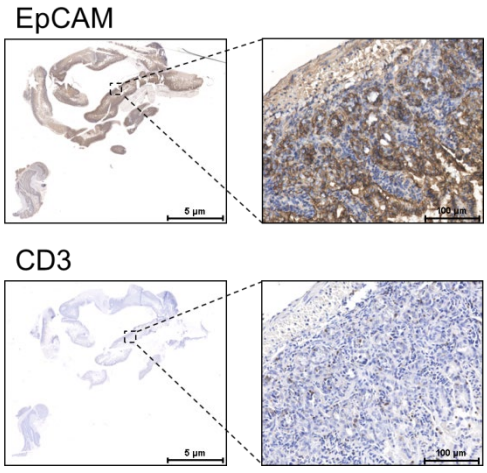

Supplementary figure 5. *Ex-vivo* macro and microscopic analysis of the duodenum from immunocompetent mice 24 hours after injection of 10 µg [^{89}Zr]Zr-DFO-*N*-suc-BiTE molecule. **A**, top panel shows an overview of the autoradiography signal. Below the

corresponding H&E stained tissue. **B**, EpCAM and CD3 staining of the duodenum showing high uniform presence of EpCAM-positive and CD3-positive cells.

Supplementary Table 1. % ID/g values from *ex-vivo* biodistribution of ^{89}Zr-muS110 (*n* = 7), ^{89}Zr-AMG 110 (*n* = 7) and ^{89}Zr-hyS110 (*n* = 7) in 4T1-tumor bearing immunocompetent mice 24 hours pi. Differences between either ^{89}Zr-AMG 110 and ^{89}Zr-hyS110 versus ^{89}Zr-muS110 were tested with a Bonferroni-corrected Mann-Whitney U test. *P*-values ≤ 0.05 are shown.

Tissue	[^{89}Zr]Zr-DFO-*N*-suc-muS110	[^{89}Zr]Zr-DFO-*N*-suc-AMG 110	Difference versus-muS110 (*P*)	[^{89}Zr]Zr-DFO-*N*-suc-hyS110	Difference versus muS110 (*P*)
Blood	0.27 (0.23 to 0.29)	0.12 (0.11 to 0.13)	0.001	0.44 (0.34 to 0.48)	0.044
Heart	1.10 (0.98 to 1.14)	1.13 (1.02 to 1.16)	0.001	1.78 (1.64 to 1.95)	0.001
Lung	1.51 (1.21 to 1.67)	1.33 (0.76 to 1.93)	n.s.	1.48 (1.16 to 1.80)	n.s.
Liver	9.18 (8.66 to 11.65)	4.71 (4.58 to 5.69)	0.002	10.94 (10.71 to 12.26)	n.s.
Pancreas	1.54 (1.19 to 1.67)	0.63 (0.56 to 0.74)	0.001	1.13 (1.01 to 1.20)	n.s.
Thymus	1.83 (1.78 to 2.26)	0.84 (0.70 to 0.90)	0.001	2.48 (2.17 to 2.69)	n.s.
Spleen	6.89 (6.74 to 8.29)	2.33 (2.18 to 2.43)	0.002	9.14 (8.72 to 10.66)	n.s.
Mesenteric LNs	3.02 (2.80 to 4.16)	1.90 (1.20 to 2.04)	0.001	6.78 (5.70 to 8.50)	0.002
Stomach	1.74 (1.55 to 2.08)	0.65 (0.57 to 0.80)	0.001	2.01 (1.81 to 2.34)	n.s.
Duodenum	3.66 (3.33 to 4.43)	0.58 (0.49 to 0.66)	0.001	2.01 (1.67 to 2.44)	0.001
Ileum	2.76 (2.45 to 3.63)	0.49 (0.40 to 0.59)	0.001	1.87 (1.82 to 2.25)	0.04
Colon	1.00 (0.87 to 1.24)	0.61 (0.58 to 0.65)	0.008	1.14 (1.04 to 1.51)	n.s.
Muscle	0.25 (0.19 to 0.27)	0.22 (0.19 to 0.26)	n.s.	0.39 (0.36 to 0.48)	0.008
Bone	0.96 (0.95 to 1.10)	0.60 (0.59 to 0.66)	0.001	0.70 (0.57 to 1.07)	n.s.
Bone marrow	3.41 (2.43 to 7.07)	4.17 (3.76 to 4.96)	n.s.	3.86 (2.84 to 7.81)	n.s.
Skin	0.93 (0.70 to 1.22)	0.88 (0.60 to 1.11)	n.s.	1.17 (1.12 to 1.30)	n.s.
Brain	0.02 (0.02 to 0.03)	0.02 (0.02 to 0.03)	n.s.	0.02 (0.02 to 0.04)	n.s.
Tumor	1.96 (1.39 to 2.61)	2.13 (1.92 to 2.21)	n.s.	2.66 (2.51 to 3.18)	n.s.
Kidney	58.24 (57.07 to 67.49)	150.57 (143.26 to 182.62)	0.001	72.30 (70.53 to 81.45)	n.s.

Supplementary Table 2. % ID/g values from *ex-vivo* biodistribution of [^{89}Zr]Zr-DFO-*N*-suc-muS110 (*n* = 4) and [^{89}Zr]Zr-DFO-*N*-suc-AMG 110 (*n* = 5) in 4T1-tumor bearing immunodeficient mice 24 hours pi. Differences between [^{89}Zr]Zr-DFO-*N*-suc-muS110 and [^{89}Zr]Zr-DFO-*N*-suc-AMG 110 and were tested with a Mann-Whitney U test. *P*-values ≤ 0.05 are shown.

Tissue	[^{89}Zr]Zr-DFO-*N*-suc-muS110	[^{89}Zr]Zr-DFO-*N*-suc-AMG 110	Difference (*P*)
Blood	0.13 (0.10 to 0.18)	0.20 (0.09 to 0.24)	n.s.
Heart	0.71 (0.60 to 0.80)	1.03 (0.94 to 1.18)	n.s.
Lung	2.05 (1.32 to 2.71)	0.69 (0.60 to 1.50)	n.s.
Liver	5.79 (4.57 to 6.80)	4.54 (4.06 to 4.65)	n.s.
Pancreas	1.06 (0.96 to 1.10)	0.46 (0.45 to 0.57)	0.032
Spleen	3.37 (2.62 to 3.76)	1.51 (1.19 to 1.55)	n.s.
Mesenteric LNs	1.67 (1.24 to 2.07)	1.52 (1.23 to 1.77)	n.s.
Stomach	0.92 (0.83 to 0.97)	0.55 (0.50 to 0.56)	0.016
Duodenum	1.61 (1.48 to 1.73)	0.52 (0.44 to 0.56)	0.016
Ileum	1.31 (1.22 to 1.48)	0.42 (0.41 to 0.46)	0.016
Colon	0.70 (0.63 to 0.74)	0.64 (0.59 to 0.66)	n.s.
Muscle	0.22 (0.19 to 0.25)	0.27 (0.21 to 0.31)	n.s.
Bone	0.82 (0.73 to 0.84)	0.70 (0.67 to 0.71)	n.s.
Bone marrow	1.53 (1.32 to 1.60)	2.14 (1.78 to 2.46)	n.s.
Skin	1.86 (1.66 to 2.04)	1.98 (1.59 to 2.47)	n.s.
Brain	0.01 (0.01 to 0.02)	0.02 (0.02 to 0.03)	n.s.
Tumor	1.46 (1.27 to 1.58)	1.72 (1.64 to 1.74)	n.s.
Kidney	46.43 (39.41 to 53.17)	185.91 (174.76 to 192.56)	0.016

Supplementary Table 3. % ID/g values from *ex-vivo* biodistribution of [^{89}Zr]Zr-DFO-*N*-suc-muS110 (*n* = 7) and [^{89}Zr]Zr-DFO-*N*-suc-AMG 110 (*n* = 6) in 4T1-tumor bearing immunocompetent mice 24 hours pi, after receiving 10 µg muS110 for 5 days. Differences between [^{89}Zr]Zr-DFO-*N*-suc-muS110 and [^{89}Zr]Zr-DFO-*N*-suc-AMG 110 and were tested with a Mann-Whitney U test. *P*-values ≤ 0.05 are shown.

Tissue	[^{89}Zr]Zr-DFO-*N*-suc-muS110	[^{89}Zr]Zr-DFO-*N*-suc-AMG 110	Difference (*P*)
Blood	0.33 (0.24 to 0.39)	0.31 (0.27 to 0.35)	n.s.
Heart	0.76 (0.71 to 0.95)	1.51 (1.36 to 1.54)	0.001
Lung	0.69 (0.66 to 0.83)	1.05 (0.87 to 1.33)	0.041
Liver	7.28 (5.56 to 8.60)	5.33 (4.65 to 6.40)	n.s.
Pancreas	0.73 (0.51 to 0.90)	0.88 (0.72 to 0.95)	n.s.
Thymus	2.02 (1.51 to 2.21)	1.83 (1.47 to 1.95)	n.s.
Spleen	4.15 (3.92 to 5.07)	1.53 (1.26 to 1.83)	0.001
Mesenteric LNs	1.89 (1.70 to 2.38)	1.87 (1.53 to 2.57)	n.s.
Stomach	0.85 (0.83 to 1.02)	1.02 (0.86 to 1.17)	n.s.
Duodenum	1.46 (1.34 to 1.72)	1.00 (0.87 to 1.15)	0.022
Ileum	1.24 (1.02 to 1.45)	1.62 (1.34 to 2.02)	n.s.
Colon	0.64 (0.61 to 0.75)	1.17 (0.82 to 1.37)	0.022
Muscle	0.18 (0.15 to 0.23)	0.22 (0.19 to 0.29)	n.s.
Bone	1.07 (0.95 to 1.23)	1.06 (0.99 to 1.21)	n.s.
Bone marrow	1.76 (1.40 to 2.07)	1.78 (1.58 to 1.99)	n.s.
Skin	0.92 (0.79 to 1.12)	1.60 (1.33 to 2.25)	0.014
Brain	0.02 (0.02 to 0.03)	0.02 (0.02 to 0.02)	n.s.
Tumor	1.38 (1.09 to 1.43)	1.89 (1.82 to 2.00)	0.001
Kidney	65.01 (52.31 to 67.98)	142.74 (137.14 to 157.45)	0.001

Supplementary Table 4. % ID/g values from ex-vivo biodistribution comparing 10 µg [^{89}Zr]Zr-DFO-*N*-suc-muS110 to immunocompetent mice (*n* = 7), immunodeficient mice (*n* = 4) and repeated mus110 administration mice (*n* = 7), 24 hours pi. Differences between either the immunodeficient mice and the repeated muS110 administration group versus the immunocompetent mice were tested with a Bonferroni-corrected Mann-Whitney U test. *P*-values ≤ 0.05 are shown.

Tissue	[^{89}Zr]Zr-DFO-*N*-suc-muS110 (immunocompetent)	[^{89}Zr]Zr-DFO-*N*-suc-muS110 (Immunodeficient)	Difference versus immunocompetent (*P*)	[^{89}Zr]Zr-DFO-*N*-suc-muS110 (repeated dosing)	Difference versus immunocompetent (*P*)
Blood	0.27 (0.23 to 0.29)	0.13 (0.10 to 0.18)	n.s.	0.33 (0.24 to 0.39)	n.s.
Heart	1.10 (0.98 to 1.14)	0.71 (0.60 to 0.80)	0.024	0.76 (0.71 to 0.95)	n.s.
Lung	1.51 (1.21 to 1.67)	2.05 (1.32 to 2.71)	n.s.	0.69 (0.66 to 0.83)	0.002
Liver	9.18 (8.66 to 11.65)	5.79 (4.57 to 6.80)	0.024	7.28 (5.56 to 8.60)	n.s.
Pancreas	1.54 (1.19 to 1.67)	1.06 (0.96 to 1.10)	n.s.	0.73 (0.51 to 0.90)	0.004
Spleen	6.89 (6.74 to 8.29)	1.67 (1.24 to 2.07)	0.012	4.15 (3.92 to 5.07)	0.001
Mesenteric LNs	3.02 (2.80 to 4.16)	0.92 (0.83 to 0.97)	0.012	1.89 (1.70 to 2.38)	0.001
Stomach	1.74 (1.55 to 2.08)	1.61 (1.48 to 1.73)	0.024	0.85 (0.83 to 1.02)	0.004
Duodenum	3.66 (3.33 to 4.43)	1.31 (1.22 to 1.48)	0.012	1.46 (1.34 to 1.72)	0.001
Ileum	2.76 (2.45 to 3.63)	0.70 (0.63 to 0.74)	0.012	1.24 (1.02 to 1.45)	0.001
Colon	1.00 (0.87 to 1.24)	0.22 (0.19 to 0.25)	n.s.	0.64 (0.61 to 0.75)	0.022
Muscle	0.25 (0.19 to 0.27)	0.82 (0.73 to 0.84)	n.s.	0.18 (0.15 to 0.23)	n.s.
Bone	0.96 (0.95 to 1.10)	1.53 (1.32 to 1.60)	n.s.	1.07 (0.95 to 1.23)	n.s.
Bone marrow	3.41 (2.43 to 7.07)	1.86 (1.66 to 2.04)	0.012	1.76 (1.40 to 2.07)	0.014
Skin	0.93 (0.70 to 1.22)	0.01 (0.01 to 0.02)	0.024	0.92 (0.79 to 1.12)	n.s.
Brain	0.02 (0.02 to 0.03)	1.46 (1.27 to 1.58)	n.s.	0.02 (0.02 to 0.03)	n.s.
Tumor	1.96 (1.39 to 2.61)	46.43 (39.41 to 53.17)	n.s.	1.38 (1.09 to 1.43)	n.s.
Kidney	58.24 (57.07 to 67.49)	0.13 (0.10 to 0.18)	0.048	65.01 (52.31 to 67.98)	n.s.

Supplementary Table 5. % ID/g values from ex-vivo biodistribution comparing 10 µg [^{89}Zr]Zr-DFO-*N*-suc-AMG 110 to immunocompetent mice (*n* = 7), immunodeficient mice (*n* = 4) and repeated mus110 administration mice (*n* = 6), 24 hours pi. Differences between either the immunodeficient mice and the repeated muS110 administration group versus the immunocompetent mice were tested with a Bonferroni-corrected Mann-Whitney U test. *P*-values ≤ 0.05 are shown.

Tissue	[^{89}Zr]Zr-DFO-*N*-suc-AMG 110 (immunocompetent)	[^{89}Zr]Zr-DFO-*N*-suc-AMG 110 (Immunodeficient)	Difference versus immunocompetent (*P*)	[^{89}Zr]Zr-DFO-*N*-suc-AMG 110 (repeated dosing)	Difference versus immunocompetent (*P*)
Blood	0.12 (0.11 to 0.13)	0.20 (0.09 to 0.24)	n.s.	0.31 (0.27 to 0.35)	0.002
Heart	1.13 (1.02 to 1.16)	1.03 (0.94 to 1.18)	n.s.	1.51 (1.36 to 1.54)	0.044
Lung	1.33 (0.76 to 1.93)	0.69 (0.60 to 1.50)	n.s.	1.05 (0.87 to 1.33)	n.s.
Liver	4.71 (4.58 to 5.69)	4.54 (4.06 to 4.65)	n.s.	5.33 (4.65 to 6.40)	n.s.
Pancreas	0.63 (0.56 to 0.74)	0.46 (0.45 to 0.57)	n.s.	0.88 (0.72 to 0.95)	n.s.
Spleen	2.33 (2.18 to 2.43)	1.51 (1.19 to 1.55)	0.017	1.53 (1.26 to 1.83)	0.017
Mesenteric LNs	1.90 (1.20 to 2.04)	1.52 (1.23 to 1.77)	n.s.	1.87 (1.53 to 2.57)	n.s.
Stomach	0.65 (0.57 to 0.80)	0.55 (0.50 to 0.56)	n.s.	1.02 (0.86 to 1.17)	n.s.
Duodenum	0.58 (0.49 to 0.66)	0.52 (0.44 to 0.56)	n.s.	1.00 (0.87 to 1.15)	0.028
Ileum	0.49 (0.40 to 0.59)	0.42 (0.41 to 0.46)	n.s.	1.62 (1.34 to 2.02)	0.002
Colon	0.61 (0.58 to 0.65)	0.64 (0.59 to 0.66)	n.s.	1.17 (0.82 to 1.37)	0.016
Muscle	0.22 (0.19 to 0.26)	0.27 (0.21 to 0.31)	n.s.	0.22 (0.19 to 0.29)	n.s.
Bone	0.60 (0.59 to 0.66)	0.70 (0.67 to 0.71)	n.s.	1.06 (0.99 to 1.21)	0.002
Bone marrow	4.17 (3.76 to 4.96)	2.14 (1.78 to 2.46)	n.s.	1.78 (1.58 to 1.99)	n.s.
Skin	0.88 (0.60 to 1.11)	1.98 (1.59 to 2.47)	0.005	1.60 (1.33 to 2.25)	0.022
Brain	0.02 (0.02 to 0.03)	0.02 (0.02 to 0.03)	n.s.	0.02 (0.02 to 0.02)	n.s.
Tumor	2.13 (1.92 to 2.21)	1.72 (1.64 to 1.74)	0.034	1.89 (1.82 to 2.00)	n.s.
Kidney	150.57 (143.26 to 182.62)	185.91 (174.76 to 192.56)	n.s.	142.74 (137.14 to 157.45)	n.s.